Marchant AL, Billam TP, Yu MMH, Rakonjac A, Helm JL, Polo J, Weiss C, Gardiner SA, Cornish SL.

Date deposited:

12/04/2016

Quantum reflection of bright solitary matter waves from a narrow attractive potential

A. L. Marchant,[1] T. P. Billam,[1] M. M. H. Yu,[1] A. Rakonjac,[1] J. L. Helm,[1] J. Polo,[2] C. Weiss,[1]
S. A. Gardiner,[1] and S. L. Cornish[1,*]

[1]*Joint Quantum Centre (JQC) Durham-Newcastle, Department of Physics, Durham University, Durham DH1 3LE, United Kingdom*
[2]*Department de Física, Universitat Autònoma de Barcelona, E-08193 Bellaterra, Spain*

We report the observation of quantum reflection from a narrow attractive potential using bright solitary matter waves formed from a ^{85}Rb Bose-Einstein condensate. We create the attractive potential using a tightly focused, red-detuned laser beam, and observe reflection of up to 25% of the atoms, along with the confinement of atoms at the position of the beam. We show that the observed reflected fraction is much larger than theoretical predictions for a simple Gaussian potential well. A more detailed model of bright soliton propagation, accounting for the generic presence of small subsidiary intensity maxima in the red-detuned beam, suggests that these small intensity maxima are the cause of this enhanced reflection.

Solitons are nondispersive and self-localized waves that arise when nonlinear interactions are sufficient to balance dispersion. Since the first observations in shallow water [1], extensive studies of such solitary wave solutions have been carried out in a diverse range of fields, including nonlinear optics and optical fibers [2–4], plasma physics [5], and magnetism [6]. In the context of quantum gases, quasi-one-dimensional (1D) Bose-Einstein condensates (BECs) may be well described by the homogeneous 1D Gross-Pitaevskii equation (GPE), a nonlinear Schrödinger equation that manifests exact soliton solutions [7]. Experimentally, a quasi-1D limit is typically approached by confining the condensate in a highly elongated trap with tight radial confinement and weak axial confinement. While this precludes mathematically exact soliton solutions, the resulting solitary wave solutions retain many characteristics of the ideal soliton [8–10], such as propagation without dispersion and stability in collisions. For the more typical case of repulsive interatomic interactions, *dark* solitary waves are observed [11,12]. However, for attractive interatomic interactions one observes *bright* solitary waves; nondispersive BEC wave packets that are free to propagate over macroscopic distances. Previous experimental work has realized both single and multiple bright solitary matter waves using ^{7}Li atoms [13–15] and ^{85}Rb atoms [16–18], stimulating intense theoretical interest (see [10], and references therein).

Scattering of bright solitary matter waves from narrow *repulsive* potential barriers has been extensively studied theoretically [19–24]. The nature of the scattering depends crucially on the center-of-mass kinetic energy of the solitary wave relative to the modulus of its ground state energy [25]. For high kinetic energies the barrier can act as a beam splitter; the outcome of recombining the two resulting solitary waves depends strongly on their relative phase [26] (as recently experimentally demonstrated [27]), potentially allowing one to realize a matter-wave interferometer [19]. For low kinetic energies, the scattering can produce quantum superposition states [25,28,29]. Previous theoretical studies

have also addressed the scattering of bright solitary waves from narrow *attractive* potential wells, where the possibility exists for the bright solitary wave to undergo quantum reflection. Significant quantum reflection has been predicted for low energy solitons [30], along with significant resonant trapping when the attractive potential supports bound states [31]. Quantum reflection of atoms and molecules has previously been observed from solid surfaces [32,33], reflection gratings [34], and liquid helium [35]. However, quantum reflection of matter waves from an attractive *optical* potential allows one to also observe transmission and, potentially, trapping of the matter waves.

In this Rapid Communication, we report the observation of splitting and quantum reflection of a bright solitary matter wave from a narrow attractive potential formed from a tightly focused, red-detuned laser beam. We investigate how the fraction of atoms reflected varies with the depth of the attractive potential, and observe atoms confined at the position of the well. Surprisingly, we measure much greater reflected fractions than can be explained by theoretical predictions for a Gaussian potential well. We address this discrepancy via extensive theoretical modeling using the GPE, providing strong evidence that the presence of small subsidiary diffraction maxima in the red-detuned beam, creating a multiple-well structure, is the main source of the enhanced reflection. While small subsidiary diffraction maxima are generically expected and commonly observed in tightly focused beams, our experiment is unusual in that they cause qualitative changes in behavior. Our results suggest that carefully engineered attractive multiwell potentials may make robust beam splitters for solitary wave interferometry.

We create stable ^{85}Rb condensates using the method described in [36]. Our setup uses a levitated crossed optical dipole trap [37] providing independent control of the trapping frequencies (dominated by the optical confinement) and the magnetic bias field used to tune the scattering length. In order to avoid the large negative background scattering length and the associated collapse instability [38–40], we use the broad Feshbach resonance at 155 G between atoms in the $F = 2$, $m_F = -2$ state to tune the scattering length to positive values. Close to the resonance the s-wave scattering length
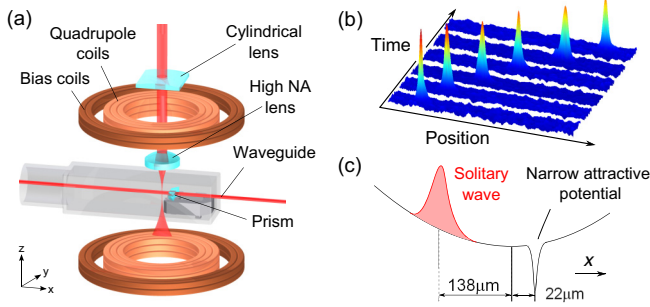
---
*s.l.cornish@durham.ac.uk

FIG. 1. (a) Experimental setup. Atoms are cooled in a crossed optical dipole trap (not shown), and then transferred into an optical waveguide. Additional axial confinement is provided by magnetic quadrupole and bias fields. The narrow attractive potential is formed using a high numerical aperture (NA) lens to produce a light sheet, tightly focused in the x direction. (b) Absorption images of solitary wave propagation in the optical waveguide. (c) Schematic showing the position of the narrow attractive potential, relative to the trap center and the initial position of the solitary wave.

takes the form

$$a_s = a_{\text{bg}}\left(1 - \frac{\Delta}{B - B_{\text{peak}}}\right), \qquad (1)$$

where $a_{\text{bg}} = -443(3)a_0$, $\Delta = 10.71(2)$ G, and $B_{\text{peak}} = 155.041(18)$ G [41]. This allows us to tune the scattering length with a sensitivity $\sim 40\,a_0\,\text{G}^{-1}$ close to the zero crossing at 165.75 G. Experimentally the magnetic field is calibrated by driving rf transitions between neighboring m_F states. We produce nearly pure condensates of up to 4×10^4 atoms at a scattering length of $a_s \approx 200a_0$ in an almost spherical trapping geometry with $\omega_{x,y,z} = 2\pi[30(1),30(1),42(2)]$ Hz. The condensate number is reduced to ~ 6000 atoms by further evaporation to facilitate solitary wave production.

In each run of the experiment we create a single solitary wave [17] by releasing the BEC from the crossed dipole trap [37,42] into an optical waveguide [see Fig. 1(a)] and simultaneously tuning to a negative scattering length using the Feshbach resonance [41]. The optical waveguide provides radial confinement, but leaves the solitary wave free to propagate in the axial direction. We find that a scattering length of $a_s = -7a_0$ (where a_0 is the Bohr radius) minimizes the dispersion of the condensate as it travels along the waveguide [see Fig. 1(b)] while also avoiding the collapse instability [38–40]. Motion in the axial direction is due to a weak harmonic potential that results from the combination of the magnetic bias field, B_z, used to access the Feshbach resonance and the magnetic gradient, B_z', used to levitate the atoms. This is given by $\omega_x = 1/2\sqrt{\mu B_z'^2/mB_z}$, where μ is the magnetic moment of the atoms, and m their mass [42]. This magnetic potential dominates the weak (< 0.1 Hz) optical potential of the waveguide in the axial direction. The overall trapping frequencies in the waveguide are $\omega_{x,y,z} = 2\pi[1.15(5),18.2(5),18.2(5)]$ Hz.

Crucially the position of the magnetic potential minimum with respect to the position of the crossed dipole trap can be precisely controlled, thereby offering control of the motion of the solitary wave in the waveguide. The maximum velocity of
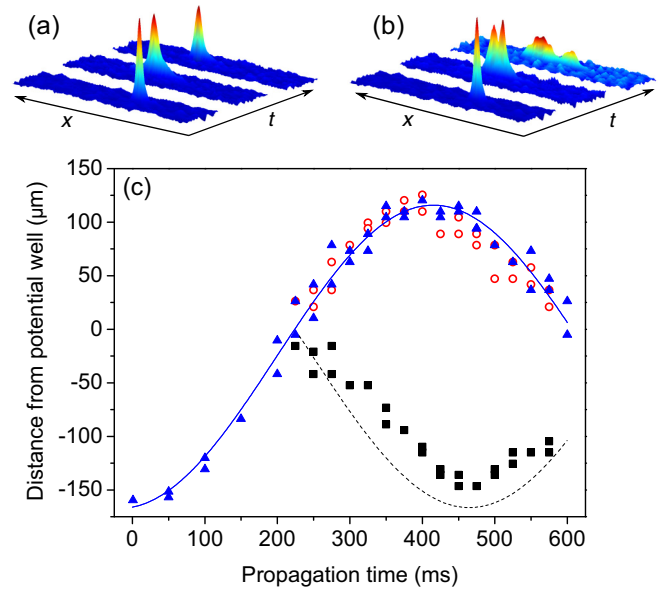

FIG. 2. Splitting of the solitary wave. Absorption images showing the low velocity propagation of the solitary wave (a) without and (b) with the attractive well present at 1, 250, and 500 ms. (c) In the absence of the well (blue triangles) the atoms oscillate in the waveguide. With the well present the solitary wave splits, with atoms being both transmitted (red circles) and reflected (black squares). Lines indicate classical trajectories for free propagation (solid) and elastic reflection (dashed).

the wave packet is given simply by $v_{\text{max}} = A\omega_x$ where ω_x is the trapping frequency and A is the amplitude of the motion, i.e., the distance between the crossed dipole trap and the minimum of the magnetic potential. We introduce a narrow attractive potential well using $\lambda = 852$ nm light, focused to form a light sheet with beam waists of $w_x = 1.9(2)\,\mu\text{m}$ and $w_y = 570(40)\,\mu\text{m}$ (determined by parametric heating of thermal atoms trapped at the focus of the beam). At full power we obtain a maximum well depth of $1\,\mu\text{K} \times k_B$. We position the potential well $\sim 22\,\mu\text{m}$ from the minimum of the axial waveguide potential and release the solitary wave from the crossed dipole trap situated $\sim 160\,\mu\text{m}$ away from the well [as shown in Fig. 1(c)], giving an incident velocity of $\sim 1\,\text{mm s}^{-1}$ [43].

In our initial experiment we set the potential well depth to its maximum value, release a solitary wave into the waveguide, and track its position by imaging multiple instances of the same experimental sequence at different times after release (see Fig. 2). All images of the atomic clouds are taken using destructive absorption imaging with a resonant probe beam propagating along the y axis [44]. Once the solitary wave reaches the well, we observe a splitting of the wave packet and identify three distinct resulting fragments: atoms transmitted, reflected, and confined at the potential well. We are able to track the center-of-mass positions of both the transmitted and reflected atomic clouds, as shown in Fig. 2(c). The majority of atoms in the solitary wave are transmitted (red circles), following the same trajectory as in the freely propagating case (blue triangles), undergoing harmonic motion in the waveguide (solid line). Up to 10% of the atoms appear to be confined close to the well. The remainder of the atoms
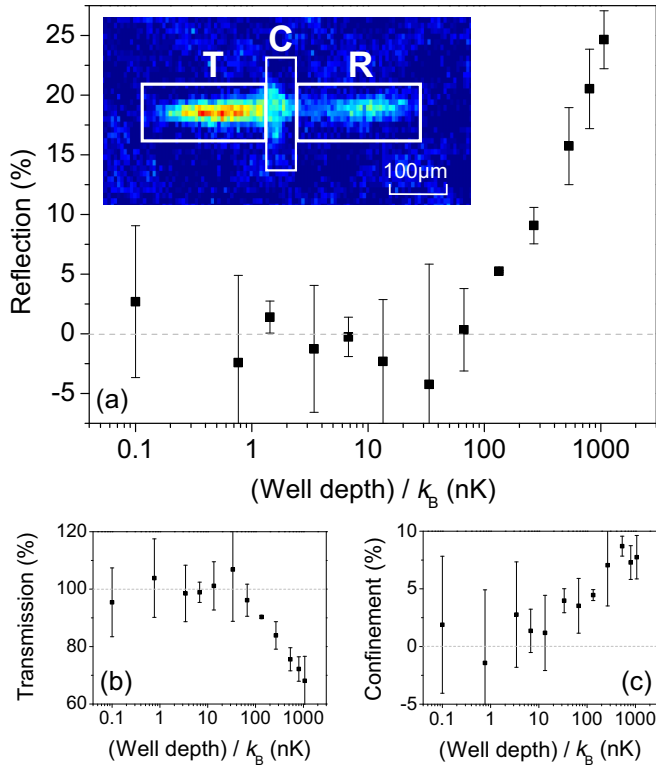
FIG. 3. The percentage (a) reflection (R), (b) transmission (T), and (c) confinement (C), of atoms as a function of well depth for an incident solitary wave with a velocity of 1 mm s^{-1}. These percentages are determined using regions defined in the inset of (a) (see text for details).

($\sim$25%) reflect from the narrow potential well and propagate in the opposite direction to the transmitted component. The turning point of the reflected atoms occurs $\sim$50 ms later than for the transmitted atoms due to the offset of the well position from the trap center. This turning point is $\sim$20 μm short of the release position, suggesting some energy is lost during the splitting process. It is likely that this is in fact transferred into radial excitations and/or heating of the resultant clouds [45] (cf. [22]). For comparison, the trajectory of an elastic collision is shown by the dashed line in Fig. 2(c).

To explore the effect of the potential well depth relative to the kinetic energy of the incoming solitary wave we vary the power of the 852 nm beam, while keeping all other parameters constant. The solitary wave is split and the resulting fragments allowed to spatially separate before they are imaged, 475 ms after release. To calculate the reflection probability, we define three fixed regions of the absorption images: transmitted (T), confined (C), and reflected (R), as shown in the inset of Fig. 3(a). Taking the sum of the pixel values in each of these regions we define the reflection probability as R/(R + C + T) × 100%. Values for the transmitted and confined parts are calculated similarly. We find there is no observable reflection from the narrow potential well for trap depths <100 nK. Above this threshold, the probability of reflection increases sharply [see Fig. 3(a)], and the number of atoms transmitted drops correspondingly [Fig. 3(b)]. For a trap depth of 1 μK × k_B, we observe a reflection of $\sim$25%.

The number of atoms confined at the position of the well also increases with increasing well depth, as shown in Fig. 3(c).

In the splitting experiments reported we observe the width of the transmitted and reflected clouds to be larger than the original solitary wave. However, due to the low amplitude of the atomic motion (138 μm) and weak (1 Hz) confinement along the waveguide beam it is difficult to spatially separate the atomic clouds following their interaction with the well. This fact, coupled with limited resolution of the imaging system, means we are unable to reliably fit a Gaussian line shape to the images, and are thus unable to report a quantitative figure for the increase in width. Qualitatively, however, we see an increase in the size of the transmitted and reflected components which is significantly greater than the expected change for a ground state soliton where, in the mean-field description, the width scales inversely with the atom number [7]. This raises the question as to whether the solitary waves survive the interaction with the potential well. We also note that the atoms which appear to be confined at the position of the well have a larger radial size than the reflected and transmitted clouds. This spreading is reminiscent of the expansion of thermal atoms along a tightly focused dipole trapping beam [at full power, the well has $\omega_{x,y,z} \simeq 2\pi(1500,25,120)$ Hz]. Considering the relative trapping frequencies of the waveguide and light sheet, it is plausible that the strong compression of the cloud of atoms confined in the light sheet increases the temperature to the point where the atoms may overcome the radial confinement of the waveguide ($\sim$600 nK) leading to the observed vertical spreading in the images. This conversion of energy from kinetic to thermal could potentially explain the reduced amplitude of the reflected atoms observed in Fig. 2.

Intriguingly, the observed reflection [Fig. 3(a)] is too large to be explained by quantum reflection from a simple Gaussian potential well of the form

$$V_G(x) = -V_0 \exp(-2x^2/\ell^2), \qquad (2)$$

where $V_0 > 0$ and $\ell = 1.9$ μm. A simple approximate argument for this comes from the analytic formula for the single-particle reflection coefficient for the similar potential $V(x) = -V_0/\cosh^2(x/d)$ (choosing $d \approx \ell/1.6$) [46],

$$R = \frac{\cos^2(\pi\sqrt{1/4 + 2mV_0d^2/\hbar^2})}{\sinh^2(\pi kd) + \cos^2(\pi\sqrt{1/4 + 2mV_0d^2/\hbar^2})}, \qquad (3)$$

where k is the wave vector of the incoming plane wave. Since $\cos^2(x) \leqslant 1$ for all real arguments x, this approximation shows that for $\ell = 1.9$ μm a small incoming velocity (small k) is necessary to observe any reflection, *regardless of the well depth* V_0. For velocities v ≈ 1 mm s^{-1}, as realized in the experiment, this approximation predicts negligible reflection ($\sim$0.006%). Indeed, for this velocity a well with a depth of 1 μK × k_B would require $\ell = 0.44$ μm to realize the 25% reflection seen in the experiment.

The lack of substantial reflection predicted by the analytic single-particle expression [Eq. (2)] is confirmed by detailed numerical simulations of a quasi-one-dimensional GPE

$$i\hbar\frac{\partial\psi(x,t)}{\partial t} = \left[\frac{-\hbar^2}{2m}\frac{\partial^2}{\partial x^2} + V(x) + U(x,t) - g_{1D}|\psi(x,t)|^2\right]$$
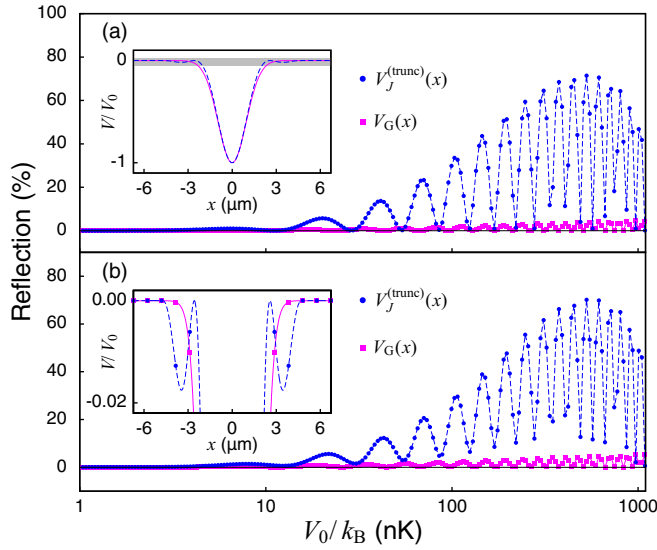$$\times \psi(x,t), \qquad (4)$$

FIG. 4. Extreme variation in predicted reflection for small changes in spatial structure of the potential. Main panels show calculated reflection coefficients as a function of potential depth for (a) noninteracting wave packets ($a_s = 0$) and (b) bright solitary waves ($a_s = -7a_0$) in a 1D GPE model. Results are shown for both Gaussian [$V_G(x)$], and truncated diffraction-pattern [$V_J^{(\text{trunc})}(x)$] potentials. The inset to (a) shows the large-scale similarity between these potentials. The inset to (b) shows the subsidiary potential wells [zoom of gray area in inset to (a)]; these have $\lesssim 2\%$ the depth of the main well, but strongly influence the reflectivity.

where $U(x,t)$ represents the time-dependent background trapping potential. We model this potential as

$$U(x,t) = \tfrac{1}{2}m[\omega_{x_1}(t)^2(x - x_1)^2 + \omega_{x_2}(t)^2(x - x_2)^2], \quad (5)$$

where $x_1 = -160\ \mu$m ($x_2 = -22\ \mu$m) represents the location of the minimum of the dipole (waveguide) potential in x [see Fig. 1(c)]. The trap frequencies for these potentials are ramped linearly over the first $\tau = 250$ ms: $\omega_{x_1}(t) = \max\{2\pi\nu_1(\tau - t)/\tau, 0\}$ and $\omega_{x_2}(t) = \min\{2\pi\nu_2 t/\tau, 2\pi\nu_2\}$, for $\nu_1 = 30$ Hz and $\nu_2 = 1.15$ Hz. The (static) potential well $V(x)$ is centered on $x = 0$ in these coordinates, and the atoms move towards positive x. The nonlinearity $g_{1D} = 4\pi N|a_s|\hbar\nu_\perp$, where we take $N = 6000$ and $\nu_\perp = 18.2$ Hz. We work with $\psi(x,t)$ normalized to unity, and initialize the simulation with $\psi(x,t)$ in the ground state of the system for potential $U(x,t = 0)$.

In agreement with the approximate formula [Eq. (3)], these simulations confirm that only very weak reflection ($\lesssim 4\%$) is expected from the Gaussian potential, both for noninteracting wave packets [Fig. 4(a)], and for bright solitary waves [Fig. 4(b)]. We have confirmed that these results are not significantly changed by the use of a three-dimensional (3D) GPE model, either with or without the inclusion of additional noise in the initial wave packet.

To qualitatively explain the surprisingly large observed reflection we consider the effects of subsidiary diffraction maxima in the optical intensity. These occur generically in focusing optical configurations [47] but, since they are generally much less intense than the primary maximum, they are typically ignored when modeling optical potentials in BEC experiments. However, in the context of our experiment,
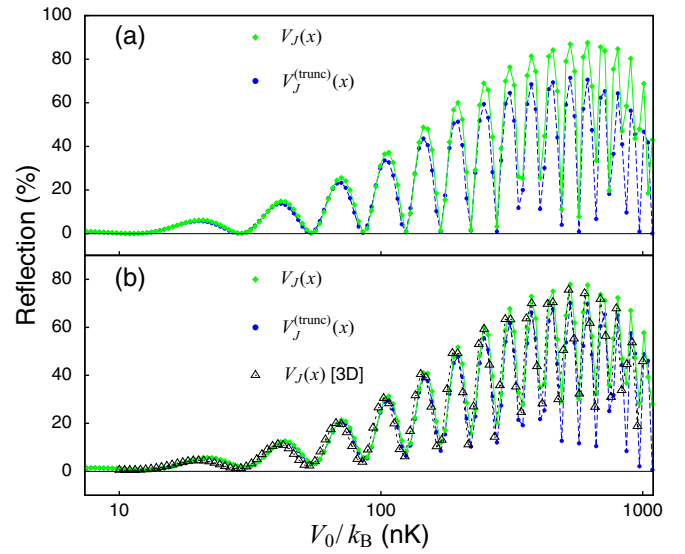

FIG. 5. Comparison of 1D GPE predictions for the reflection between potentials $V_J^{(\text{trunc})}(x)$ and $V_J(x)$ (see text) for (a) noninteracting wave packets ($a_s = 0$) and (b) bright solitary waves ($a_s = -7a_0$). Also shown in (b) are results of a 3D GPE simulation with equivalent parameters.

the *narrow* nature of the subsidiary maxima is potentially significant; at least when considered in isolation, they are able to produce larger reflection than the primary maximum [Eq. (3) predicts $\sim 0.06\%$ reflection for the first subsidiary maximum alone]. Crucially, the presence of multiple potential wells can significantly enhance reflection; this is seen, for example, in Bragg reflection of BECs from a multiple-well lattice [48].

While the exact structure of the subsidiary diffraction maxima in the red-detuned beam is not precisely known in our experiment, as a generic model we consider the first pair of subsidiary potential minima due to the intensity pattern of Fraunhofer diffraction from an aperture [47], giving the potential

$$V_J^{(\text{trunc})}(x) = \begin{cases} V_J(x), & |2\sqrt{2}x/\ell| < \alpha_2 \\ 0, & |2\sqrt{2}x/\ell| \geqslant \alpha_2, \end{cases} \quad (6)$$

where

$$V_J(x) = -V_0\left[\frac{\ell}{\sqrt{2}x}J_1\left(\frac{2\sqrt{2}x}{\ell}\right)\right]^2, \quad (7)$$

and α_2 is the second positive zero of the Bessel function $J_1(x)$. As shown in Fig. 4 (inset) this potential has the same form as $V_G(x)$ when viewed at large scales, but also a pair of subsidiary minima. The results of 1D GPE simulations for both noninteracting wave packets [Fig. 4(a)] and for bright solitary waves [Fig. 4(b)] show that the reflection is greatly enhanced for this potential compared to $V_G(x)$ over the range of well depths used in the experiment. The presence of subsidiary diffraction maxima in the beam producing the potential well thus provides a plausible explanation for the substantial reflection probabilities observed in the experiment. We obtain very similar results for the potential $V_J(x)$ [see Fig. 5(a)], indicating that the high-amplitude and oscillatory

structure of the reflection coefficient can be considered as a transmission resonance effect attributable to the three central potential wells. We have also confirmed that these results are not significantly changed by the use of a cylindrically symmetric 3D GPE model as shown in Fig. 5(b).

Unsurprisingly, there are quantitative differences between the experimental data [Fig. 3(a)] and our generic model; in particular, the model exhibits negligible ($< 1\%$) confinement, and an oscillatory structure not seen in the experiment. Our simulations have excluded small shot-to-shot changes in the incoming soliton velocity due to small ($\sim \pm 5~\mu$m) shifts in the alignment of the experimental potentials as an explanation for the latter. We therefore suspect that the quantitative differences arise from two main effects: first, the exact structure of the potential well is unlikely to be captured precisely by our generic model. Secondly, the previously noted vertical spreading of the confined fraction observed in the experiment suggests that the compression of the atomic cloud as it passes through the potential well may cause significant heating; this would likely lead to incoherent, finite-temperature dynamics not captured by our GPE model.

In summary, we have observed quantum reflection of a bright solitary matter wave from a narrow attractive potential, formed by a tightly focused laser beam. Reflection probabilities of up to 25% are measured, with the remaining atoms either transmitted or confined at the position of the potential well. Modeling of the system suggests that the exact spatial form of the potential well is crucial in determining the amount of reflection observed, with the presence of multiple optical diffraction maxima, rather than a single Gaussian maximum, playing an essential role. These results indicate that carefully engineered attractive multiwell potentials, readily generated

using spatial light modulators [49], could be developed as robust beam splitters for use in solitary wave interferometry. Here the narrow, self-trapped nature of the solitary waves makes them ideal for measuring the transmitted and reflected fractions of a wave packet incident on a beam splitter [19,20,23,24]. To further explore the splitting process we plan to modify our apparatus to allow the 1 Hz curvature along the waveguide to be removed, or even reversed, giving greater control over the spatial separation of the resultant wave packets. This will allow quantitative measurements of the cloud size after splitting to be made, giving a definitive answer as to whether the solitary waves persist following their interaction with the potential well. This is of key importance for interferometry applications. In future work we plan to replace the focused laser beam with a room-temperature superpolished glass prism (shown in Fig. 1), allowing us to explore quantum reflection due to the attractive Casimir-Polder potential [50].

The data presented in this paper are freely available to download [51].

[1] J. Scott Russell, *Report of the Fourteenth Meeting of the British Association for the Advancement of Science* (John Murray, London, 1845), p. 311.

[2] L. F. Mollenauer, R. H. Stolen, and J. P. Gordon, Phys. Rev. Lett. **45**, 1095 (1980).

[3] Y. V. Kartashov, B. A. Malomed, and L. Torner, Rev. Mod. Phys. **83**, 247 (2011).

[4] Y. S. Kivshar and G. Agrawal, *Optical Solitons: From Fibers to Photonic Crystals* (Elsevier Science, San Diego, 2003).

[5] K. Stasiewicz, P. K. Shukla, G. Gustafsson, S. Buchert, B. Lavraud, B. Thidé, and Z. Klos, Phys. Rev. Lett. **90**, 085002 (2003).

[6] Y. Togawa, Y. Kousaka, S. Nishihara, K. Inoue, J. Akimitsu, A. S. Ovchinnikov, and J. Kishine, Phys. Rev. Lett. **111**, 197204 (2013).

[7] P. Kevrekidis, D. Frantzeskakis, and R. Carretero-González, *Emergent Nonlinear Phenomena in Bose-Einstein Condensates* (Springer, New York, 2008).

[8] L. D. Carr and Y. Castin, Phys. Rev. A **66**, 063602 (2002).

[9] T. P. Billam, S. A. Wrathmall, and S. A. Gardiner, Phys. Rev. A **85**, 013627 (2012).

[10] T. P. Billam, A. L. Marchant, S. L. Cornish, S. A. Gardiner, and N. G. Parker, in *Spontaneous Symmetry Breaking, Self-Trapping, and Josephson Oscillations*, edited by B. A. Malomed, Progress in Optical Science and Photonics Vol. 1 (Springer, New York, 2013), p. 403.

[11] S. Burger, K. Bongs, S. Dettmer, W. Ertmer, K. Sengstock, A. Sanpera, G. V. Shlyapnikov, and M. Lewenstein, Phys. Rev. Lett. **83**, 5198 (1999).

[12] J. Denschlag, J. E. Simsarian, D. L. Feder, C. W. Clark, L. A. Collins, J. Cubizolles, L. Deng, E. W. Hagley, K. Helmerson, W. P. Reinhardt, S. L. Rolston, B. I. Schneider, and W. D. Phillips, Science **287**, 97 (2000).

[13] L. Khaykovich, F. Schreck, G. Ferrari, T. Bourdel, J. Cubizolles, L. D. Carr, Y. Castin, and C. Salomon, Science **296**, 1290 (2002).

[14] K. E. Strecker, G. B. Partridge, A. G. Truscott, and R. G. Hulet, Nature (London) **417**, 150 (2002).

[15] P. Medley, M. A. Minar, N. C. Cizek, D. Berryrieser, and M. A. Kasevich, Phys. Rev. Lett. **112**, 060401 (2014).

[16] S. L. Cornish, S. T. Thompson, and C. E. Wieman, Phys. Rev. Lett. **96**, 170401 (2006).

[17] A. L. Marchant, T. P. Billam, T. P. Wiles, M. M. H. Yu, S. A. Gardiner, and S. L. Cornish, Nat. Commun. **4**, 1865 (2013).

[18] G. D. McDonald, C. C. N. Kuhn, K. S. Hardman, S. Bennetts, P. J. Everitt, P. A. Altin, J. E. Debs, J. D. Close, and N. P. Robins, Phys. Rev. Lett. **113**, 013002 (2014).

[19] J. L. Helm, T. P. Billam, and S. A. Gardiner, Phys. Rev. A **85**, 053621 (2012).

[20] A. D. Martin and J. Ruostekoski, New J. Phys. **14**, 043040 (2012).

[21] J. Cuevas, P. G. Kevrekidis, B. A. Malomed, P. Dyke, and R. G. Hulet, New J. Phys. **15**, 063006 (2013).

[22] J. Polo and V. Ahufinger, Phys. Rev. A **88**, 053628 (2013).

[23] J. L. Helm, S. J. Rooney, C. Weiss, and S. A. Gardiner, Phys. Rev. A **89**, 033610 (2014).

[24] J. L. Helm, S. L. Cornish, and S. A. Gardiner, Phys. Rev. Lett. **114**, 134101 (2015).

[25] B. Gertjerenken, T. P. Billam, L. Khaykovich, and C. Weiss, Phys. Rev. A **86**, 033608 (2012).

[26] N. G. Parker, A. M. Martin, S. L. Cornish, and C. S. Adams, J. Phys. B **41**, 045303 (2008).

[27] J. H. V. Nguyen, P. Dyke, D. Luo, B. A. Malomed, and R. G. Hulet, Nat. Phys. **10**, 918 (2014).

[28] C. Weiss and Y. Castin, Phys. Rev. Lett. **102**, 010403 (2009).

[29] A. I. Streltsov, O. E. Alon, and L. S. Cederbaum, Phys. Rev. A **80**, 043616 (2009).

[30] C. Lee and J. Brand, Europhys. Lett. **73**, 321 (2006).

[31] T. Ernst and J. Brand, Phys. Rev. A **81**, 033614 (2010).

[32] F. Shimizu, Phys. Rev. Lett. **86**, 987 (2001).

[33] T. A. Pasquini, Y. Shin, C. Sanner, M. Saba, A. Schirotzek, D. E. Pritchard, and W. Ketterle, Phys. Rev. Lett. **93**, 223201 (2004).

[34] B. S. Zhao, G. Meijer, and W. Schöllkopf, Science **331**, 892 (2011).

[35] J. J. Berkhout, O. J. Luiten, I. D. Setija, T. W. Hijmans, T. Mizusaki, and J. T. M. Walraven, Phys. Rev. Lett. **63**, 1689 (1989).

[36] A. L. Marchant, S. Händel, S. A. Hopkins, T. P. Wiles, and S. L. Cornish, Phys. Rev. A **85**, 053647 (2012).

[37] D. Jenkin, D. McCarron, M. Köppinger, H. Cho, S. Hopkins, and S. Cornish, Eur. Phys. J. D **65**, 11 (2011).

[38] P. A. Ruprecht, M. J. Holland, K. Burnett, and M. Edwards, Phys. Rev. A **51**, 4704 (1995).

[39] J. L. Roberts, N. R. Claussen, S. L. Cornish, E. A. Donley, E. A. Cornell, and C. E. Wieman, Phys. Rev. Lett. **86**, 4211 (2001).

[40] E. A. Donley, N. R. Claussen, S. L. Cornish, J. L. Roberts, E. A. Cornell, and C. E. Wieman, Nature (London) **412**, 295 (2001).

[41] N. R. Claussen, S. J. J. M. F. Kokkelmans, S. T. Thompson, E. A. Donley, E. Hodby, and C. E. Wieman, Phys. Rev. A **67**, 060701 (2003).

[42] Y.-J. Lin, A. R. Perry, R. L. Compton, I. B. Spielman, and J. V. Porto, Phys. Rev. A **79**, 063631 (2009).

[43] The ratio of kinetic energy to ground state energy for this velocity is ~ 46, putting us in the high kinetic energy regime.

[44] Ideally the atoms would be imaged *in situ*, however, here a 2 ms time of flight is used to allow switching off of the large bias field. However, this time of flight is short on the time scales of the waveguide trapping frequencies such that the images effectively show the *in situ* density distribution.

[45] T. P. Billam, S. L. Cornish, and S. A. Gardiner, Phys. Rev. A **83**, 041602 (2011).

[46] L. D. Landau and E. M. Lifshitz, *Quantum Mechanics: Non-Relativistic Theory*, 3rd ed., Course of Theoretical Physics Vol. 3 (Butterworth-Heinemann, Oxford, 1977), Sec. 25.

[47] M. Born and E. Wolf, *Principles of Optics*, 4th ed. (Pergamon, Oxford, 1970).

[48] C. M. Fabre, P. Cheiney, G. L. Gattobigio, F. Vermersch, S. Faure, R. Mathevet, T. Lahaye, and D. Guéry-Odelin, Phys. Rev. Lett. **107**, 230401 (2011).

[49] G. D. Bruce, M. Y. H. Johnson, E. Cormack, D. A. W. Richards, J. Mayoh, and D. Cassettari, J. Phys. B **48**, 115303 (2015).

[50] S. L. Cornish, N. G. Parker, A. M. Martin, T. E. Judd, R. G. Scott, T. M. Fromhold, and C. S. Adams, Physica D (Amsterdam) **238**, 1299 (2009).

[51] A. L. Marchant, T. P. Billam, M. M. H. Yu, A. Rakonjac, J. L. Helm, J. Polo, C. Weiss, S. A. Gardiner, and S. L. Cornish, Quantum Reflection of Bright Solitary Matter Waves from a Narrow Attractive Potential: Supporting Data, doi:10.15128/cc24b379-1be2-4c42-862b-8895aa495968 (2015).